Residual stress simulation and measurement of Fe-Mn-Si shape memory alloy coating

Ju Heng, Lin Chengxin, Zhang Jiaqi, Liu Zhijie

(Transportation Equipments and Ocean Engineering College, Dalian Maritime University, Dalian 116026, China)

Abstract: To prepare a low-residual-stress laser cladding coating, Fe-Mn-Si shape memory alloy(SMA) coating was prepared on the surface of the AISI 304 stainless steel. And the ANSYS finite element software was used to simulate its stress field, meanwhile the residual stress distribution of the cladding specimens was measured by the mechanical hole-drilling method under the same process to verify the correctness of simulation. What′s more, the mechanism of low residual stress inside Fe-Mn-Si SMA coating was analyzed by XRD. The results show that the stress caused by laser cladding induces the $\gamma \rightarrow \varepsilon$ martensite phase transition inside the coating to get a low residual stress coating. And the coating alternately bears the thermal stress of tensile-pressure-tensile during laser spot getting closer and further to the coating center. And the thermal stress was inversely proportional to the distance between the simulating nodes and the center of laser heat source. When the specimen was completely cooled to the room temperature, the residual stress inside coating presented tensile stress, and its maximum value happened at the junction between the substrate and the coating. In the directions of parallel and vertical to the laser scanning, stress value was relatively small in the middle region, but large in two sides. And from the coating peak to the fusion line in the thickness direction, the residual stress was tensile stress and the extreme value of stress was locating at the center of the coating. Far away from the fusion line, the substrate bore pressure stress and levels off to zero-stress state.

Key words: laser cladding; residual stress; Fe-Mn-Si SMA coating; numerical simulation; hole-drilling method

CLC number: TG174.445 **Document code:** A **DOI:** 10.3788/IRLA201746.1017009

Fe-Mn-Si 形状记忆合金涂层残余应力模拟与测量

鞠 恒,林成新,张佳琪,刘志杰

(大连海事大学 交通运输装备与海洋工程学院,辽宁 大连 116026)

摘 要: 为制备低残余应力涂层，在 304 不锈钢表面激光熔覆 Fe-Mn-Si 形状记忆合金涂层。采用 ANSYSTM 有限元分析软件分析其应力场，利用机械钻孔法测量相同工艺条件下的激光熔覆试样的残余应力分布特性对模拟结果进行验证，并采用 XRD 分析 Fe-Mn-Si 记忆合金涂层低残余应力机理。结果表明,激光熔覆产生的应力诱发 Fe-Mn-Si 记忆合金各涂层 $\gamma \rightarrow \varepsilon$ 马氏体转变,将残余应力释

收稿日期: 2017-02-09； **修订日期:** 2017-03-12

基金项目: 中央高校基本科研业务费专项基金(3132016354)

作者简介: 鞠恒(1990-),男,博士生,主要从事激光加工方面的研究。Email:jh1990@dlmu.edu.cn

导师简介: 林成新(1963-),男,教授,博士,主要从事 Fe 基记忆合金及激光加工方面的研究。Email:lchxin@dlmu.edu.cn

放,得到低残余应力涂层。在受到各道激光照射(光斑接近至远离)过程中产生的热应力交替呈现为“拉-压-拉”应力状态,越远离激光热源中心,热应力越小;冷却完成后,激光涂层上残余应力表现为拉应力,最大应力位于基体与涂层交界处;在垂直与平行于激光熔覆两个方向上,涂层中的残余应力均呈现两侧大中间小的分布规律,在厚度方向上,熔覆涂层表面至涂层中心残余拉应力逐渐增加到最大值后,过涂层中心至熔化边界残余拉应力的数值开始逐渐降低,过涂层边界后,基体承受压应力并逐渐趋于零应力应力状态。

关键词:激光熔覆; 残余应力; Fe-Mn-Si 形状记忆合金涂层; 数值模拟; 钻孔法

0 Introduction

Laser cladding is a technique melting two or more kinds of materials by the way of laser heating to obtain the coating which possesses material respective properties [1]. Compared with traditional surface modification process, the laser cladding can produce much better coatings. The coating possesses fine grain, high bonding strength and low dilution because of its rapid heating, cooling rate and concentrated laser energy in the process. Meanwhile, the laser cladding can deposit high-performance materials on high-value component made by different base materials to enhance its surface properties, for instance, the resistance against corrosion, wear, and high-temperature oxidation. What′ s more, the application of the laser cladding in repairing large-scale machines and precious metals can also save material resources, efficiently.

Nevertheless, due to the insufficient replenishment of the liquid metal in the cooling process and the constraint of the substrate in the shrink process, the residual stresses generated during the cladding process. Sometimes the deformation and crack caused by the residual stress are harmful to the performance and the useful life of the products [2]. Thus, it has great significance to relieve the residual stress inside coating in detail.

And the residual stress value of the coating should be represented firstly to testify the stress′s decrease. The experimental methods, such as laboratory X -ray, synchrotron diffraction and hole-drilling method, are often used to measure the stress value. But laser cladding is a complicated chemical and physical process, which is influenced by the technology of laser cladding, the geometry size of sample and the surface state of substrate. Thus, difficulties and high cost often accompany with most experimental methods. With the high development of technology, the ANSYS finite element software is often adopted to numerically simulate the stress field of coating[3].

In this study, a low residual stress Fe -Mn -Si SMA coating was prepared on the surface of the 304 stainless steel due to coating´s exceptional property. Fe-Mn-Si SMA coating can relax the residual stress by using the stress as a driving force to induce the $\gamma \rightarrow \varepsilon$ martensite phase transition [4]. Meanwhile, the value and distribution of residual stress in the Fe -Mn -Si SMA coating model were numerically simulated by ANSYSTM, and the mechanical hole-drilling method (inexpensive and easily-operated) was used to verify the accuracy of simulation results.

1 Simulation and experiment

1.1 Finite element model

1.1.1 Heat source model

Considering the uneven distribution of the laser energy inside the laser spot(more in the middle region and little in the edge), Gauss model (Eq.(1))[5] was always used because of its heat flux distribution. To simulate the metallurgical bonding between the powder and the substrate during the moving process of the

simulating source, the APDL programming language and the Birth-Death feature were chosen.

$$q(r)=q_m\exp\left(-\frac{3r^2}{R^2}\right),\ q_m=\frac{3r^2}{R^2}Q,\ Q=\eta P \qquad (1)$$

Wherein, q_m is the maximum heat flux, $J\cdot m^{-2}\cdot s^{-1}$; R is the effective radius of arc, mm; r is the radial distance from the center of laser beam, mm. Q is the laser effective power, W; η is the efficiency of the laser cladding power; P is the laser cladding power, W.

1.1.2 Material characteristic parameters

In the model, the thermal and mechanical fields were sequentially coupled. That is, the temperature field inside the material during all process was computed first with a transient thermal analysis, and the temperature field results were given as a static load for the stress field analysis. The parameters for simulating the temperature and the stress field should fully define. The thermo-physical parameters defined for the temperature field simulation include: heat conductivity coefficient, density specific heat and enthalpy; The physics parameters defined for the stress field include: thermal expansion coefficient, Poisson ration, elasticity modulus, shear modulus, and yield strength. The composition of the 304 stainless steel (Cr 18.14, Ni 8.71, Mn 1.148, Si 0.404, C 0.069, Fe Bal.) and the Fe-Mn-Si SMA coating (Cr 10.98, Ni 4.97, Mn 16.25, Si 5.89, Fe Bal.) were measured by multi-channel spark direct reading spectrometer. Table 1 and Tab.2 clearly show the material properties of the Fe-Mn-Si SMA coating and the 304 stainless steel, which were taken from reference [6] and JMatpro software.

Tab.1 Properties of Fe-Mn-Si SMA

Temperature/℃	20	100	300	500	800	1 200	1 300	1 450	1 800
Density/kg·m^{-3}	7 870	7 493	7 383	7 271	7 069	6 761	6 483	6 389	6 031
Thermal conductivity/W·m^{-1}·K^{-1}	14.7	15.7	18.5	21.3	25.0	28.9	27.8	30.0	35.4
Specific heat/J·kg^{-1}·K^{-1}	495	502	539	575	757	703	4 672	812	848
Coefficient of linear expansion/10^{-5}·K^{-1}	2.37	2.40	2.47	2.53	2.82	3.24	4.24	4.46	5.68
Enthalpy value/J·g^{-1}	−154	−117	−13	98	295	617	858	1 012	1 306
Elastic modulus/10^{10}·Pa	17.89	17.39	16.00	14.51	11.86	7.992	0.046	0	0
Poisson ration	0.296	0.299	0.306	0.314	0.325	0.341	0.476	0.5	0.5
Yield strength/10^{8}·Pa	6.37	5.70	5.12	4.08	2.03	0.12	0.01	0	0
Shear modula/10^{9}·Pa	69.00	66.93	61.21	55.20	44.74	29.79	0.015	0	0

Tab.2 Properties of 304 stainless steel

Temperature/℃	20	100	300	500	800	1 200	1 300	1 450	1 800
Density/kg·m^{-3}	8 020	7 950	7 860	7 750	7 645	7 530	7 300	6 900	6 615
Thermal conductivity/W·m^{-1}·K^{-1}	14.85	18.41	22.41	26.41	30.41	34.41	42.41	36.54	50.41
Specific heat/J·kg^{-1}·K^{-1}	449	502	562	1026	617	634	919	5011	839
Coefficient of linear expansion/10^{-5}·K^{-1}	1.65	1.77	1.83	1.9	1.97	–	2.08	–	2.10
Enthalpy Value/J·g^{-1}	107	191	297	418	559	687	973	1 106	1 480
Elastic modulus/10^{10}·Pa	20.5	19.5	17.8	15.9	13.6	11.8	7.49	0.42	0
Poisson ration	0.295	0.308	0.320	0.335	0.345	0.365	0.375	0.45	0.45
Yield strength/10^{8}·Pa	1.80	1.30	1.08	0.82	0.69	–	0.63	0.60	0
Ultimate tensile strength/10^{8}·Pa	5.86	4.96	4.39	3.50	2.00	0.57	0.54	0.50	0

1.1.3 Geometric model

The three-dimensional finite element model was established to simulate the value and distribution characteristics of the residual stress in the cladding specimens. The length, width, height of substrate is 100, 50, 10 mm, and these dimensions of coating is 90, 30, 1.5 mm. And the coating was successively lapped by nineteen single tracks along the *X*-direction (Fig.1(b)). Meanwhile, the mesh adapted to the model is graphically shown in Fig.1(a), and the element size decreases from the zone of the coating to the borders of the plates. To ensure the computation precision and save the calculation time, most parts of the model were meshed with quadratic except the multi-track coating zone, and the units of the coating and substrate are SOLID90 and SOLID70, respectively.

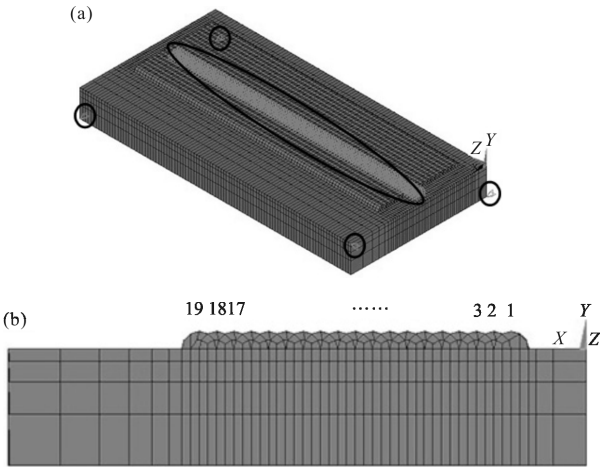

Fig.1 Displacement constraint (a) and mesh generation (b) of the finite element model

1.1.4 Boundary conditions of temperature field and stress field

The boundary conditions of temperature field include radiation, convection and conduction. The radiation coefficient was coupled into the convective heat transfer coefficient, and the coupled coefficient was applied to the surface of model to simulate the radiation and the convection between the substrate and the ambient medium, in the end the heat conduction was considered by defining material thermal conductivity.

And the boundary condition of the stress field is a degree of freedom (displacement constraints in the three directions) in the model. The displacement constraints in *X*, *Y*, *Z* directions implemented on three vertices of the substrate and the bottom surface of coating to limit the rigid displacement of model and avoid the stress concentration[7], shown in Fig.1(a).

1.2 Sample preparation

In the laser cladding experiments, a CO_2 laser (DL-LPM-V, Dalu laser group, China, maximum power of 5 kW, wavelength 10.6 μm) was used for the material processing. And the self-made Fe/Mn/Si/Cr/Ni mixed powders whose mass ration is 53:32:9:4:2 and size range of 10-50 μm was mixed by a horizontal bowl mill for 4 h, and then placed in a vacuum drying oven at the temperature of 120 ℃ for 4 h. The wrought 304 stainless with a thickness of about 10 mm, was utilized as a substrate for laser cladding. Under the process conditions(the laser power of 2.5 kW, the laser spot diameter of 3 mm, the traverse speed of 800 mm/min, the overlap of 50% and the focal distance of 330 mm), Fe-16Mn-6Si-11Cr-5Ni SMA low residual stress coating was prepared.

1.3 Measurement of residual stress

The hole-drilling method whose standard was established in 1981 by the American Society of Testing Materials (ASTM) was used to measure the residual stress in the clad specimen. The distribution of the strain gauge is shown in Fig.2(a), and the the principal stress value was calculated by Eq.(2).

$$\begin{cases}\sigma_1=E(\varepsilon_1+\varepsilon_3)/4A-E\sqrt{(\varepsilon_1-\varepsilon_3)^2+(2\varepsilon_2-\varepsilon_1-\varepsilon_3)^2}\,4B\\ \sigma_2=E(\varepsilon_1+\varepsilon_3)/4A+E\sqrt{(\varepsilon_1-\varepsilon_3)^2+(2\varepsilon_2-\varepsilon_1-\varepsilon_3)^2}\,4B\\ \tan 2\theta=(2\varepsilon_2-\varepsilon_1-\varepsilon_3)/(\varepsilon_3-\varepsilon_1)\end{cases} \quad (2)$$

Where, ε_1, ε_2 and ε_3 are the strain measuring in three directions, respectively. σ_1 and σ_2 are the maximum and the minimum residual principal stress, respectively. θ is the included angle between the direction of σ_1 and the reference axis of No.1 strain gauge. E is the material elasticity modulus. A and B are the stress release coefficients, and they are related to

the diameter, the depth of drilling hole and the size of the strain rosette. The stress release coefficients are measured with CB3395–92 standard, and the value are –0.276e–12(GPa)$^{-1}$ and–0.567e–12(GPa)$^{-1}$, respectively.

In the test, the bit diameter (D_0), the drilling depth (h) and the distance (D) between the center of the drilling hole and the edge of the strain gage is 1.5, 1.8, 5 mm, respectively. The laser cladding specimen corresponding to the model was also lapped with nineteen single coatings, and Fig.2(b) shows the topography of surface and the distribution of measuring points in the hole-drilling method. The strain value was measured with a mean value method that reads strain value each 5 minutes within 35 minutes after drilling and calculates the mean strain. The six measuring points are parallel to the laser scanning direction and have a separation distance of 15 mm. The position of No.1 measure point is 10 mm away from coating′s bottom edge and 12.5 mm away from the substrate′s left margin.

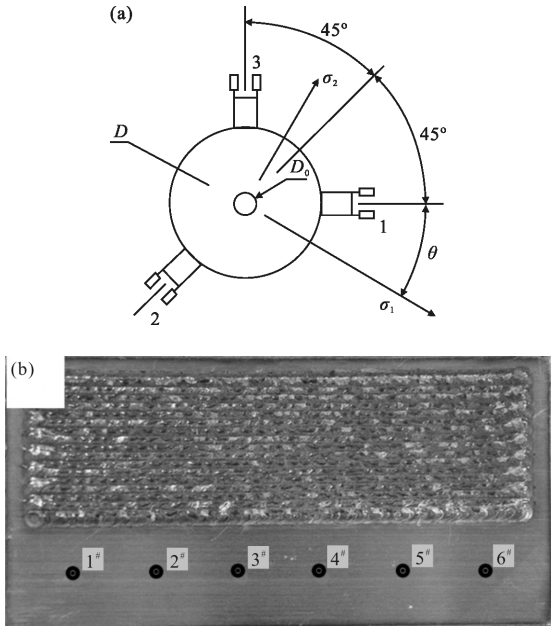

Fig.2 Arrangement of strain gage (a) and diagram of measuring points distribution (b)

2 Results and discussion

2.1 Residual stress analysis during the laser cladding process

Figure 3(a)–(d) illustrate the principal stress curves of some representative (first, second, tenth and nineteenth) coating centers during the laser cladding process.

As shown in Fig.3(a), the center of the first coating alternately bears the stress of tensile-pressure-tensile during the laser spot getting closer and further to the coating, and the changing law fit the variation rule of the heat stress during the laser cladding process. When the laser spot moves to the second coating center, the first coating center locates at the edge of the laser heat source and alternately bears the tensile-pressure-tensile thermal stress for second time. The temperature gradient of the simulative point reduces when the point passes from the center to the edge of the laser spot, and the stress value is simultaneously decreasing. Then, the stress value of the coating center will level off and finally present positive in the process of cooling to the room temperature.

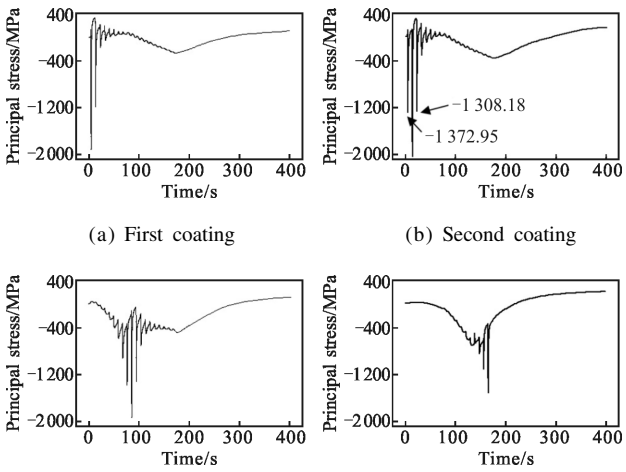

(a) First coating (b) Second coating

(c) Tenth coating (d) Nineteenth coating

Fig.3 Principal stress curves of some representative coating centers

The variation rule of the stress in the second coating center (Fig.3(b)) is basically similar to that of the first coating center. When the laser irradiates the first and the third coating centers, the simulating node (the second coating center) locates at the edge of the laser spot, and the flux of the simulating node is equal. However, the time for the laser spot irradiating from the start point to the first coating center is less, so the time for the heat treatment when the laser spot

irradiates the third coating center is longer. Because the time for the heat treatment is in inversely proportional to the residual stress value, the principal stress of simulating node at the former time (−1 372.95 MPa) is higher than the latter time(−1 308.18 MPa).

Figure 3(c)−(d) show that the stress value of the tenth and the nineteenth coating centers are zero in the initial stage of the laser cladding due to the Birth-Death feature. After the preheating and irradiaton of the laser cladding, the powders begin to fuse and bear stress. And during the melting and the cooling processes of the tenth coating center, its changing law is similar to that of the first and second coating center. The nineteenth coating center doesn′t present stress fluctuation after direct irradiation, because the coating is the last coating.

Figure 4 illustrates the major principal stress contour plots at some representative time. Figure 4(a)−(c) happens at the time of the laser spot heating the first, the second and the nineteenth coating centers, respectively. And Fig.4(d) shows the contour plot at the time when the coating cooled to the room temperature. Figure 4 indicates that only the center and the surrounding of the heat source presents the stress in the beginning stage, and the maximum stress is in the center of heat source. Then after preheating and heat conducting, most regions of the model bear major

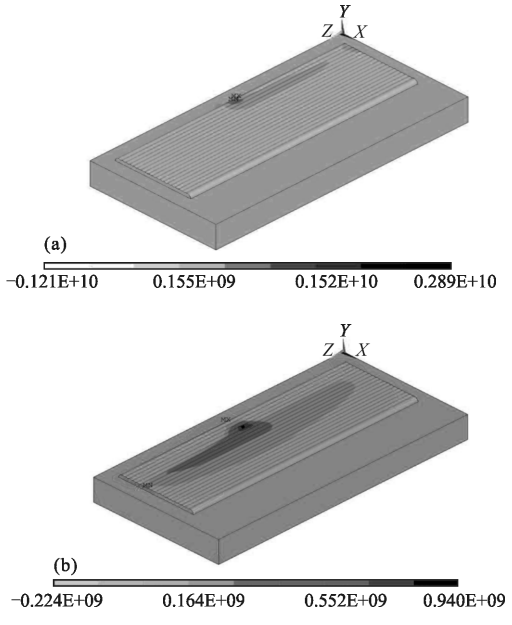

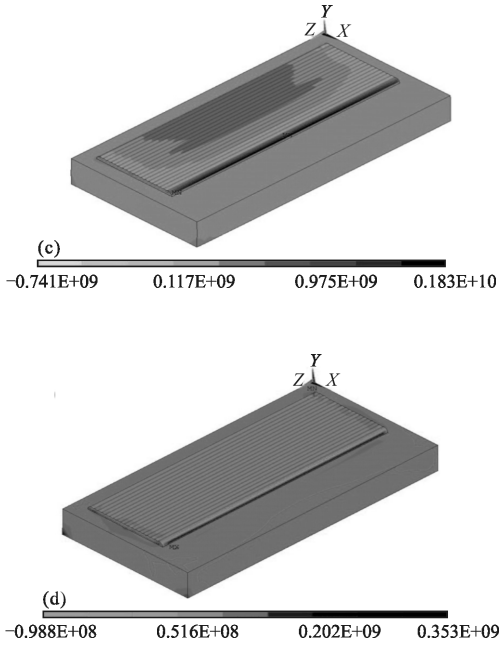

Fig.4 Major principal stress contour plots at some representative time

principal stress. And the value of the major principal stress reduces when the simulation point moves from the center to the edge of source. When the laser source moves away from the processed coating, the heat treatment reliefs the stress. Moreover, after being completely cooled, the maximum value of the stress happens at the junction between the substrate and the coating due to their different expansion coefficients. And this result is similar to what is obtained in reference [8].

2.2 Residual stress analysis after complete cooling

To research the distribution rule of the residual stress in the specimen after complete cooling, the principal stress curves of several paths were chose. The path 1 and the path 2 are the intersections of the cross-sections ($A-A$, $B-B$) and the surface of substrate. While, the cross-sections $A-A$ and $B-B$ (Fig.5(a)) are the symmetry plane of the multi-clad, which parallel and vertical to the laser scanning direction, respectively. And the principal stress curves are shown in Fig.5(b) and Fig.5(c).

As Fig.5(b) shows, the stress value reduces with the position moving from the left side of the substrate

to the edge of the first coating(point.*A* to point.*B*), as a result of the enhanced heat treatment. And the changing law is similar to that in the path from the right side of the substrate to the nineteenth coating (point.*G* to point.*F*). It is known that the residual stress is in directly proportional to the temperature gradient, and the temperature gradient is inversely proportional to the distance between the heat source and simulation point. Thus, the stress value of the simulation points decreases when the position moves from the edge of the first (point.*B*) and the nineteenth coating(point.*F*) to its center(points.*C*, *E*), respectively. The laser heat of the former coating preheats for the latter coating, and the laser heat of the latter coating applies a heat treatment for the former coating. Therefore, the temperature gradient of the middle region is lower than that of the two sides, and residual stress value presents small in the middle area (point.*D*. The "life" time of the left side coating is longer than that of the right side coating as a reason of the Birth-Death feature [9]. Thus, the heat treatment time of the left side (point.*C*) longer than the preheating time of the right side (point.*E*), the residual stress value of the former is small. Because the substrate far away from the nineteenth coating (point.*G* to point.*H*) is unmelted, the distance between simulation point and the heat source mainly influences the stress value. With the increase of the distance, the value of the stress decreases and approaches to zero gradually.

Figure 5 (c) shows that the stress increases from the edge of substrate to the center of laser spot, and the reason is similar to the changing reason of stress in the path from the edge of the first and the nineteenth coatings to their center (points.*B*, *F* to points.*C*, *E*) in the Fig.5(c). The laser is moving from the left side to the right side of the tenth coating (point.*B* to point.*D*), the "life" time of the left side point is longer. And the "life" time of the points in two sides is both lower than that in the middle region, the stress value of different regions sequence from high to low is the right region, the left region and the middle region.

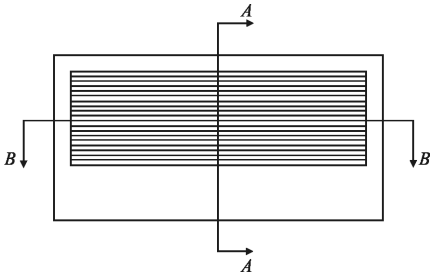

(a) Cross-sections *A*−*A* and *B*−*B*

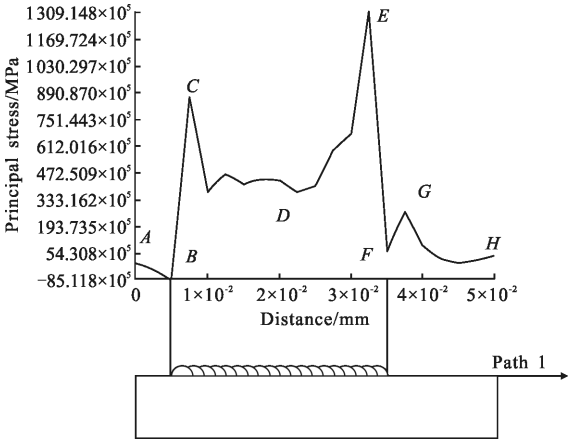

(b) In the path 1

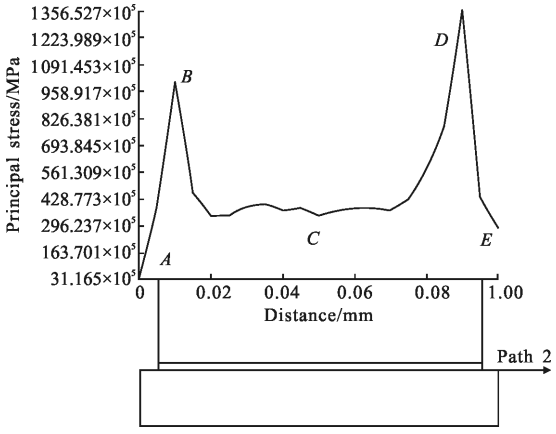

(c) In the path 2

Fig.5 Major principal stress curves in some respective paths

In order to study the distribution rule of the stress in the thickness direction of specimen, the stress curve in the path 3 which is the intersection of the tenth coating center and cross-section *C* −*C*, was chosen. The cross-section *C* −*C* crossed the tenth coating center line and in the thickness direction, as shown in Fig.6(a). And Fig.6(b) illustrates the stress

curve in the path from the surface of the coating to the bottom edge of the substrate (the null point is on the peak of coating).

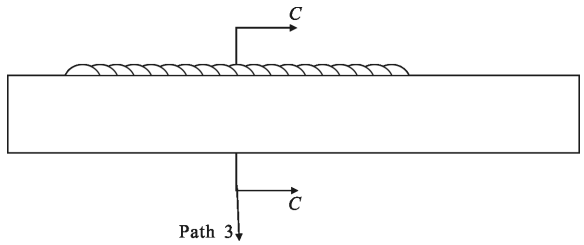

(a) Cross-section $C-C$

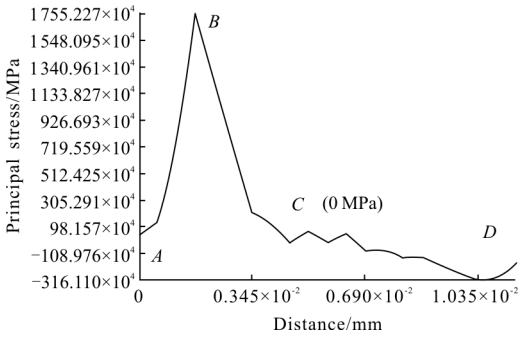

(b) In the path 3

Fig.6 Distribution of stress along the thickness of tenth cladding

The extreme value of the stress in the path 3 from the peak of the coating to the fusion line locates (point.A to point.C) at the center of coating(point.B), because its temperature gradient is higher than the other fuse zones. As a reason of the stress balance in the entire model, the unmelted substrate (point.C to point.D) present compressive stress. And the stress reduces as the distance between the simulative points and the source increase, stress value approach to zero gradually in the path from the melting boundary to the low edge, which has been highlighted in reference [10].

2.3 Results of the residual stress simulation and the hole-drilling method experiment

Figure 7 shows the principal stress value of the points measured by the hole-drilling method and the major principal strain curve simulated by the ANSYS finite element software. The path of strain curve is parallel to the laser scanning direction, and measuring points 1# and 6# were used as its two endpoints.

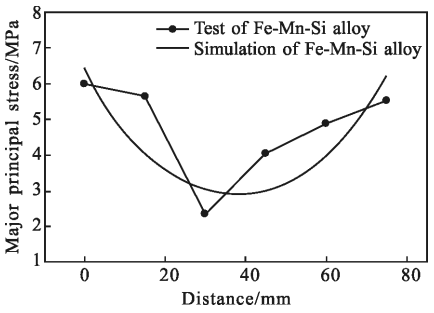

Fig.7 Major principal stress value σ_1 of the experiment and the simulation in the path

The residual stress value of measuring points is low in the middle zone, and higher in the two sides, the reason and the distribution law conforms to that of the numerical simulation. Although the stress distribution trends of the numerical simulation and the experiment possess consistency, the error still exists between their results. One of the reasons is that the Gauss heat source is an ideal heat source, but the actual laser heat source is not, which is influenced by material surface state and internal material components. Moreover, the other reason that the mesh size of model can′t match the powder also contributes to the error.

The results of the experiment and the simulation clearly show that Fe−Mn−Si SMA coating possesses low residual stress. The mechanism was inferred that the residual stress of Fe−Mn−Si SMA coating as the phase transition drive force to induce $\gamma\rightarrow\varepsilon$ martensite phase transformation, and the phase transformation relaxes the residual stress of the cladding layer.

The phase composition of Fe−Mn−Si cladding coating was analyzed by X−ray diffractometer to verify the above analysis. The X−ray diffraction pattern of Fe−Mn−Si SMA coating before and after (1 000 ℃×1 h) solid solution is shown in Fig.8.

As the Fig.8 shows, Fe−Mn−Si cladding coating exists γ austenite and ε martensite before solid solution, and only γ austenite exists after solid solution. It was indicated that $\gamma\rightarrow\varepsilon$ martensite phase transformation occurred on Fe−Mn−Si SMA coating in the laser cladding process, and residual stress of

laser cladding coating was the driving force of the phase transformation.

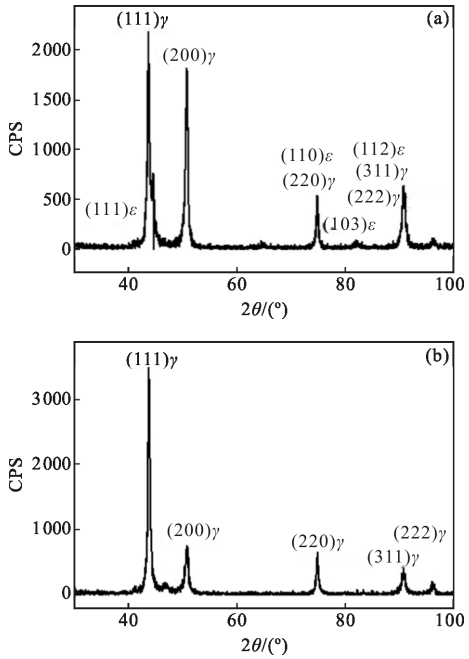

Fig.8 XRD patterns of the Fe-Mn-Si coating before (a) and after (b) solid solution

3 Conclusion

Low residual stress Fe-Mn-Si-Cr-Ni SMA coating has been produced on the surface of the AISI 304 stainless steel without additional heat treatment. The variation rules of the coating during the laser cladding process and the stress distribution in the laser cladding specimen after being complete cooled have been carried out by the ANSYSTM software. And the stress value of measuring points has been measured by the hole-drilling method to verify the validity of the simulation. Based on these studies, the following conclusions can be obtained:

(1) The multi-layer coating is formed by the way of laser successively, circularly irradiating the powder. Each coating center alternately bears thermal stress of tensile-pressure-tensile during laser spot getting closer and further. And the thermal stress is inversely proportional to the distance between the simulating node and the laser heat source center.

(2) When being completely cooled to the room temperature, the residual stress induced by the laser cladding is tensile stress, and the maximum value locates at the junction between the substrate and the coating. In the parallel and vertical direction to the laser scanning, the distribution law of the residual stress is small in the middle area, but large in the two sides. In the thickness direction, the extreme value of stress in the path from the peak of coating to the fusion line locates at the center of the coating. The stress of the unmelted substrate is compressive stress, and its value approaches to zero gradually in the path from the melting boundary to the bottom edge.

(3) The value and the distribution of the residual stress obtained by the ANSYS finite element numerical simulation and the mechanical hole-drilling method possess consistency, and the experimental results obtained by the experimental verify the accuracy of the numerical simulation.

References:

[1] Liu Hongxi, Leng Ning, Zhang Xiaowei, et al. Microstructure and wear behavior of WC/CO50 composite coating on 40Cr cutting tool surface prepared by laser cladding [J]. ***Infrared and Laser Engineering***, 2015, 44(1): 178-183. (in Chinese)

[2] Zeng Chao, Tian Wei, Liao Wenhe, et al. Study of laser cladding thermal damage: a quantified microhardness method [J]. ***Surf Coat Tech***, 2013, 236(24): 309-314.

[3] Li Jianzhong, Li Xiangfeng, Zuo Dunwen, et al. Influence of defocusing amount on the process of Al/Ti cladding above 7050 aluminum alloy based on numerical simulation study [J]. ***Infrared and Laser Engineering***, 2014, 44(4): 1126-1133. (in Chinese)

[4] Zhou Chaoyu, Lin Chengxin, Xu Peng, et al. In situ synthesis of Fe-Mn-Si memory alloy on the surface of stainless steel by laser cladding [J]. ***Rare Metal Mat Eng***, 2014, 43(12): 3042-3046. (in Chinese)

[5] Zhang Ping, Ma Lin, Zhao Junjun, et al. The heat source model of the numerical simulation in the laser cladding [J]. ***China Surface Engineering***, 2006, 19 (5): 161-164. (in Chinese)

[6] Suárez A, Amado J M, Tobar M J, et al. Study of residual stresses generated inside laser cladded plates using FEM and

diffraction of synchrotron radiation [J]. ***Surf Coat Tech***, 2010, 204(12): 1983-1988.

[7] Yang Xianqun. Predicting the quality of clad in laser cladding by powder and numerical simulation of cladding process [D]. Harbin: Harbin Institute of Technology, 2008. (in Chinese)

[8] Oliveira U D, Ocelík V, Hosson J T. Residual stress analysis in co-based laser clad layers by laboratory X-rays and synchrotron diffraction techniques[J]. ***Surf Coat Tech***, 2006, 201(3): 533-542.

[9] Bendeich P, Alam N, Brandt M, et al. Residual stress measurements in laser clad repaired low pressure turbine blades for the power industry [J]. ***Mater Sci Eng A***, 2006, 437(1): 70-74.

[10] Gu Jianqiang, Luo Fang, Yao Jianhua. Numerical simulation of residual stress during laser cladding [J]. ***Laser & Optoelectronics Progress***, 2010, 47(10): 81-86. (in Chinese)